

TIME DOMAIN VELOCITY VECTOR FOR RETRACING THE MULTIPATH PROPAGATION

Jérôme Daniel, Srđan Kitić

Orange Labs, France

ABSTRACT

We propose a conceptually and computationally simple form of sound velocity, which seamlessly exploits active and reactive sound intensity measurements, and, consequently, provides a more transparent view of acoustic multipath. We feel that this representation has a potential both as a valuable tool for directly analyzing sound propagation, as well as being a new spatial feature format for machine learning algorithms in audio and acoustics. As a showcase, we demonstrate that the Direction-of-Arrival (DoA) *and* the range of a sound source could be estimated from the First Order Ambisonics (FOA) recordings, the latter never attempted before, to the best knowledge of the authors.

Index Terms— Ambisonics, intensity, localization, DoA, distance

1. INTRODUCTION

Sound intensity is one of the most fundamental acoustic quantities, and has found its role in various applications, from coding [1], to soundfield synthesis [2, 3], psychoacoustics [4, 5] and acoustic holography [5]. Theoretically defined as an instantaneous temporal quantity, sound intensity is most often expressed in the frequency domain, assuming the harmonic decomposition of a soundfield [6]. Its real part is termed the *active intensity*, as it describes the flow of energy originating from a sound source [7, 5]. The behavior of its imaginary part, the *reactive intensity*, is somewhat less evident, as it describes the non-propagative local energy exchange that depends on the sound waves' interference [4, 8].

Narrowband active sound intensity has been widely used for sound source localization in Ambisonics, being a computationally cheap alternative to beamforming techniques [9, 1, 10, 11]. However, it has been observed [12, 13] that reverberation introduces significant bias in such DoA estimates, effectively limiting their direct use to anechoic and mildly reverberant environments. Much research has been dedicated to alleviating the multipath effects, *e.g.* by dereverberating the recorded audio [14], by exploiting the Higher Order Ambisonics (HOA) channels [15, 16], and by estimating the time-frequency bins dominated by the direct path signal [17, 18].

On the other hand, the narrowband reactive sound intensity has been largely ignored, although its physical significance has been recognized [6, 7]. A recent work [13] has shown the added value of using this quantity as an input feature for a DoA estimation neural network.

In this article, we propose a wideband representation of velocity vector [8], which naturally encapsulates both the active and reactive components of complex sound intensity. The derived features are conceptually and computationally simple, yet sufficiently rich to describe the acoustic multipath captured by an Ambisonics microphone. Indeed, as noted in several works [19, 20, 21], the acoustic reflections are not necessarily a nuisance, provided that one can identify their parameters properly.

In the following section, we model the complex sound intensity and the related velocity vector in the presence of strong acoustic reflections, and derive the Time Domain Velocity Vector (TDVV) features. In section 3 we illustrate one application of TDVV - the DoA and range estimation of a single, static sound source. Section 4 shows the experimental results obtained on the real-life Ambisonics datasets. Section 5 concludes the article.

2. TIME DOMAIN VELOCITY VECTOR

Ambisonics is a spatial audio format based on the spherical harmonic decomposition of a soundfield captured by a spherical microphone array [2, 4]. In practice, the decomposition is truncated - only a limited number of decomposition coefficients (analogously, audio channels) is retained. The FOA format keeps only four channels: the omnidirectional $w(t)$, and three figure-of-eight channels $x(t)$, $y(t)$ and $z(t)$, aligned with the coordinate axes.

The channel $w(t)$ designates the acoustic pressure $p(t)$, while the remaining three FOA channels represent its spatial derivatives (all with regards to the same point in space, *i.e.* the microphone position). Since the linearized fluid momentum equation relates the pressure gradient¹ $\vec{\nabla}p(t)$ and particle velocity $\vec{v}_p(t)$ [4], the (x, y, z) channels are proportional to particle velocity (up to multiplicative constant), *i.e.* $[x(t) \ y(t) \ z(t)]^T = \vec{\nabla}p(t) \propto \vec{v}_p(t)$. In the frequency do-

Both authors equally contributed to this work.

¹Hereafter, we use physics notation ($\vec{\cdot}$) for vector quantities, and boldface letters to denote their estimates (lowercase - vectors, uppercase - matrices).

main², we have $[X(f) Y(f) Z(f)]^T \propto \vec{V}_p(f)$.

The (frequency-domain) velocity vector (FDVV) $\vec{V}(f)$ is defined as follows³ [8, p.23]:

$$\vec{V}(f) = -\frac{1}{\rho c} \frac{\vec{V}_p(f)}{P(f)} = -\frac{j}{k} \frac{\vec{\nabla} P(f)}{P(f)} \simeq \frac{1}{W(f)} \begin{bmatrix} X(f) \\ Y(f) \\ Z(f) \end{bmatrix}, \quad (1)$$

where ρ is the specific density of air, c is the speed of sound, k is the wavenumber, and $j^2 = -1$.

The FDVV is a normalized version of *complex* sound intensity $\vec{I}(f) = P(f)\vec{V}_p(f)^*$ [6], with the distinct advantage of being less dependent on the energy $|P(f)|^2$, and thus, the content of the source signal. In the same vein, the active and reactive intensities are proportional to $\Re(\vec{V}(f))$ and $\Im(\vec{V}(f))$ [8], respectively, where $\Re(\cdot)$ and $\Im(\cdot)$ denote the real and imaginary part of a complex number.

Moreover, FDVV obeys the superposition principle, *i.e.*

$$\vec{V}(f) = \frac{\sum_n a_n \vec{u}_n}{\sum_n a_n} = \frac{\vec{u}_0 + \sum_{n \geq 1} \gamma_n \vec{u}_n}{1 + \sum_{n \geq 1} \gamma_n}. \quad (2)$$

Here a_n and \vec{u}_n are the complex magnitude and (unitary) velocity vector of the n^{th} plane wave component, respectively, while $\gamma_n = a_n/a_0$ is the relative gain of the n^{th} component with respect to the first one ($n = 0$).

Assume now a simplified setting, *i.e.* the superposition of the plane wave coming from the source direction \vec{u}_0 , and the one from the direction \vec{u}_1 (*e.g.* representing a dominant reflection, as in Fig.2). The FDVV expression (2) becomes

$$\vec{V}(f) = \frac{\vec{u}_0 + g_1(f)e^{-j2\pi f\tau_1}\vec{u}_1}{1 + g_1(f)e^{-j2\pi f\tau_1}}. \quad (3)$$

The complex gain is $\gamma_1 = g_1(f)e^{-j2\pi f\tau_1}$, where $|g_1(f)| < 1$ represents the frequency-dependent attenuation factor, and τ_1 is the corresponding propagation delay.

Since $|\gamma_1| < 1$, the expression (3) admits the expansion into the Taylor series:

$$\begin{aligned} \vec{V}(f) &= \frac{\vec{u}_0 + \gamma_1 \vec{u}_1}{1 + \gamma_1} = (\vec{u}_0 + \gamma_1 \vec{u}_1) \sum_{k \geq 0} (-\gamma_1)^k \\ &= \vec{u}_0 + \sum_{k \geq 1} (-\gamma_1)^k e^{-2\pi f k \tau_1} (\vec{u}_0 - \vec{u}_1). \end{aligned} \quad (4)$$

Approximating $g_1(f)$ by a frequency-independent constant g_1 (as, *e.g.* in [22]), and by applying the inverse Fourier transform $\mathcal{F}^{-1}(\cdot)$ to the series above, we get the TDVV $\vec{v}(t)$ for the one-reflection setting:

$$\vec{v}(t) = \mathcal{F}^{-1}(\vec{V}(f)) = \delta(t)\vec{u}_0 + \sum_{k \geq 1} \delta(t - k\tau_1) (-g_1)^k (\vec{u}_0 - \vec{u}_1). \quad (5)$$

² $S(f) = \mathcal{F}(s(t))$ denotes the Fourier representation of a signal $s(t)$.

³Without loss of generality, here we adopt the SID channel ordering with SN3D normalization [8].

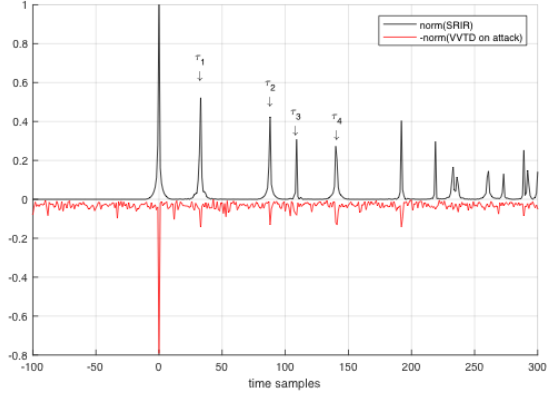


Fig. 1. The (mirrored) norm of TDVV against the (centered) norm of Room Impulse Responses of the FOA channels.

Thus, for $t > 0$ the TDVV defines a periodic sequence (with period τ_1), of alternating, exponentially decaying coefficients multiplying the difference vector $\vec{u}_0 - \vec{u}_1$. At $t = 0$, TDVV yields the unitary vector colinear with DoA, which is equal to the mean value of $\Re(\vec{V}(f))$ when the frequencies are uniformly distributed. Interestingly, it can be shown that the mode of the probability distribution of $\Re(\vec{V}(f))$ does *not* correspond to its mean. Consequently, peak-picking approaches, such as [10, 11], would suffer from a systematic bias in their DoA estimates, even under the one-reflection model.

When multiple reflections are allowed, the convergence criterion for the Taylor series becomes much more stringent, *i.e.* it translates into $|\sum_{n > 0} \gamma_n(f)| < 1, \forall f$, which implies $\sum_{n > 0} |g_n(f)| < 1$. Then, from (2) we get

$$\vec{V}(f) = \left(\vec{u}_0 + \sum_{n \geq 1} \gamma_n \vec{u}_n \right) \sum_{k \geq 0} \left(\sum_{n \geq 1} -\gamma_n(f) \right)^k. \quad (6)$$

After the inverse Fourier transform and some manipulations, the TDVV has the following form:

$$\vec{v}(t) = \delta(t)\vec{u}_0 + \sum_{n \geq 1} \sum_{k \geq 1} (-g_n)^k \delta(t - k\tau_n) (\vec{u}_0 - \vec{u}_n) + \eta. \quad (7)$$

In the expression above, we emphasized the contribution of the primary reflections, while the cross terms (interactions among the reflections themselves) are captured by the variable η . Here again, $\vec{v}(t = 0)$ reveals the source DoA, but the tail³ is now composed of a linear combination of multiple periodic series, instead of the single one, as in (5).

Unfortunately, the convergence condition above is overly restrictive in real acoustics. Empirically, we observed a rather similar behavior in the TDVV of recorded FOA signals (*cf.* Fig.1), albeit with some characteristic irregularities. The detailed analysis of the latter phenomena is left for future work.

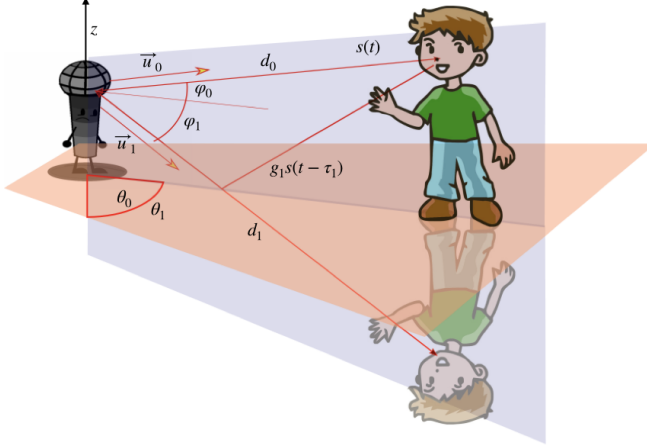


Fig. 2. Interference of the direct path and the floor reflection plane waves, by the image-source model. Note that the azimuth angles θ_0 and θ_1 are assumed equal.

3. DOA AND RANGE ESTIMATION

For a showcase application of TDVV, we propose a method to estimate the DoA and range to a sound source, using only the FOA data. The classical methods for range estimation exploit phase differences between channels and the near field propagation model, which is not feasible in our case, since the Ambisonics channels should be (theoretically) in phase. Instead, we exploit the spatial diversity provided by the one-reflection model, schematically presented in Fig.2. We assume specular reflections, and a horizontal reflecting surface - *e.g.* a floor, a table, or a ceiling.

First, we discuss the distance estimation. Provided that we have the estimates of the DoA and reflection directions (\vec{u}_0 and \vec{u}_1), as well as the propagation delay τ_1 , simple geometry states that the distances to the source and its image are related as follows:

$$d_0 \cos \varphi_0 = d_1 \cos \varphi_1,$$

where φ_0 and φ_1 are the elevation angles of \vec{u}_0 and \vec{u}_1 , respectively. Since $d_1 - d_0 = \tau_1 c$, we get the expression for the range d_0 as

$$d_0 = \frac{\tau_1 c}{\frac{\cos \varphi_0}{\cos \varphi_1} - 1}. \quad (8)$$

Hence, the goal becomes estimating the unknowns \vec{u}_0 , \vec{u}_1 and τ_1 , from the FOA recordings only. While there could be more robust ways to estimate these parameters, we choose a very simple approach that illustrates the usefulness of the TDVV representation. Indeed, assuming that the one-reflection model described in the previous section holds, the TDVV expression (5) suffices to estimate all the parameters.

The signals are processed in the Short Term Fourier Transform (STFT) domain, and estimation is done for each STFT frame independently. The FDVV is computed by the

expression (1), and assembled into the matrix $\tilde{\mathbf{V}}^{(m)}$, where m denotes the current *frame index*. While the normalization renders the FDVV more invariant to source signal's content, it may also amplify the noise within. Therefore, we run the online noise level estimator [23], and suppress the frequency bands having negative (estimated) Signal-to-Noise Ratios (SNRs). Finally, the TDVV is computed from such denoised FDVV, and represented by the matrix $\mathbf{V}^{(m)} \in \mathbb{R}^{3 \times T}$.

According to (5), the (normalized) leftmost column of $\mathbf{V}^{(m)}$ (denoted hereafter by \mathbf{u}_0), corresponds to the DoA vector \vec{u}_0 . Moreover, due to $|g_1| < 1$, for all the remaining $t > 0$, the TDVV having the largest magnitude is at the time delay $t = \tau_1$. Hence

$$\tilde{\tau}_1 = \frac{j_{\max}}{f_s}, \quad j_{\max} = \operatorname{argmax}_{j>0} \|\mathbf{V}_{:j}^{(m)}\|, \quad (9)$$

f_s is the sampling rate and $\mathbf{V}_{:j}^{(m)}$ is the j^{th} column of $\mathbf{V}^{(m)}$.

Again from (5), we deduce that $\mathbf{V}_{:j_{\max}}^{(m)}$ is colinear with $\mathbf{u}_0 - \mathbf{u}_1$, where \mathbf{u}_1 is the (unit norm) estimate of \vec{u}_1 . Thus, we immediately have

$$\mathbf{u}_1 = \mathbf{u}_0 - \frac{2 \left(\mathbf{u}_0^T \mathbf{V}_{:j_{\max}}^{(m)} \right)}{\|\mathbf{V}_{:j_{\max}}^{(m)}\|^2} \mathbf{V}_{:j_{\max}}^{(m)}. \quad (10)$$

In practice, however, even in the noiseless case, the real recordings comprise multiple reflections that may violate the single-reflection model we exploited above.

One problem are the reflections from other (non-horizontal) surfaces, and the interferences among reflections themselves (*i.e.* the cross terms in the eq. (7)). In order to suppress their contributions in the TDVV imprint, we propose to re-weight the FDVV components accordingly, *before* applying $\mathcal{F}^{-1}(\cdot)$. To determine the weights, we exploit the fact that (*cf.* Fig.2) the DoA \vec{u}_0 and the desired reflection \vec{u}_1 (as well as their difference $\vec{u}_0 - \vec{u}_1$), lie in the subspace orthogonal to the xy -plane. By examining the FDVV expression (4), we see that, for the frequency bands in which the model holds, the imaginary part $\Im(\vec{V}(f))$ is colinear with $\vec{u}_0 - \vec{u}_1$. Using the current estimate \mathbf{u}_0 , we design weights $q(f)$ as follows

$$q(f) = \exp \left(- \frac{|\Im(\tilde{\mathbf{V}}^{(m)})^T \mathbf{n}|}{\|\Im(\tilde{\mathbf{V}}^{(m)})\|} \right), \quad (11)$$

where \mathbf{n} is the unit normal to the plane defined by \mathbf{u}_0 and the z -axis. As a heuristic approach to obtain a slightly better conditioned TDVV, we apply the weighting iteratively, using the new estimate of \vec{u}_0 to compute weights each time (usually, after few iterations, the estimate stabilizes).

Another issue is that a frame could be corrupted by the impulse response tail of the preceding ones. Intuitively, the frames corresponding to signal attacks should be sufficiently energetic such that the contribution of previous acoustic propagation becomes negligible. To quantify the attack presence

in the interesting frequency bands, we use a (positive) finite difference approximation of the STFT magnitude derivative, summed channel- and frequency-wise, and weighted by $q(f)$:

$$D^{(m)} = \max \left(0, \sum_f q(f) \sum_i \frac{C(f)_i^{(m+1)} - C(f)_i^{(m-1)}}{\max(C(f)_i^{(m+1)}, C(f)_i^{(m-1)})} + \epsilon \right) \quad (12)$$

where $C(f)_i^{(m)}$ denotes the magnitude of the i^{th} FOA channel at the STFT bin (m, f) , and $\epsilon > 0$ is a small constant.

Only the frames for which $D^{(m)} \geq 0.9 \max_m D^{(m)}$ holds are preserved. Additionally, we filter out the frames for which the distance estimate $d_0^{(m)}$ is outside some reasonable limits - in our experiments, between 20cm and 5m. This is done in order to avoid heavy outliers, which may arise when the elevation cosine ratio in (8) approaches one. Indeed, in the far field setting we have $\varphi_1 \approx \varphi_0$, and the estimation becomes unstable. It is noteworthy that this is usually not an issue with vertical reflecting surfaces, such as walls. However, exploiting these requires a priori knowledge of the azimuthal orientation of the microphone.

4. RESULTS

The proposed algorithm is tested on two sets of recordings: the Task 1 development dataset of the recently proposed Acoustic Source LOCALization and TrACKing (LOCATA) challenge [12], and on our internal dataset used in the publication [13]. The LOCATA dataset is smaller than the latter, but provides the DoA and range labels, whereas the dataset in [13] contains the DoA information only. On the other hand, this one perfectly matches the considered use case - a microphone placed on the living room table. As a baseline, we used the TRAMP algorithm, presented in [10], which only exploits the active sound intensity.

The sampling frequency is 16kHz. In order to better capture the signal segments dominated by the direct propagation and horizontal echo, we use very short STFT frames ($\sim 0.005\text{s}$), and apply a 95% overlap. For TRAMP, we use the recommended frame length of 0.04s, and the same overlap size. The frame-level estimates are aggregated by median filtering, hence each algorithm outputs a unique estimate per recording (DoA, or DoA plus range).

Table 1 shows the results obtained on the three recordings comprising the LOCATA Task 1 validation dataset. In all cases, the proposed method outperforms the baseline in terms of the angular error. The average range estimation error is around 20cm (whereas the average source distance is about 2m). We conjecture that even greater gains in accuracy could be attained had we used the reflections of vertical surfaces.

Table 2 presents the mean and median angular errors for the second dataset. In addition to TRAMP, we added the results, reported in [13], of a Convolutional Recurrent Neural Network (CRNN) trained on active and reactive sound inten-

Recording	1	2	3
Angular error (TRAMP)	6.05°	8.03°	16.05°
Angular error (proposed)	3.44°	3.76°	9.17°
Range error (proposed)	32cm	13cm	18cm

Table 1. Results on the Task 1 development dataset.

Angular error	TRAMP	CRNN	Proposed
Mean	14.45°	8.1°	6.31°
Median	11.88°	5.7°	5.45°

Table 2. Results on the dataset used in [13].

sity features, provided within independent feature channels. Again, we see that the proposed algorithm largely surpasses TRAMP, and even edges out the CRNN model. This indicates that a deep neural network may benefit from the input features given in the TDVV format.

5. CONCLUSION

We presented Time Domain Velocity Vector - a novel spatial representation of Ambisonics soundfields. TDVV is almost independent of the excitation signal, and mainly encodes the propagation signature of the acoustic environment. Next, we demonstrated an application of TDVV to DoA and range estimation of an immobile sound source. Although simple, the proposed algorithm performs favorably to our baseline, strictly by exploiting the properties of the TDVV.

We postulate that these new features would enable better understanding of the multipath phenomena, from theoretical and practical perspective. For instance, this signal representation would directly benefit the methods for sound source localization and tracking, dereverberation, geometry estimation, beamforming and spatial audio coding. As a consequence, applications spanning from home and professional audio, to virtual and augmented reality, robotics and home/industrial surveillance, are easy to envision.

Future research would focus on better understanding of TDVV in more general settings, *e.g.* in the presence of multiple sources, non-specular reflections, frequency-dependant gains, or when the Taylor series expansion is not viable. From the algorithmic point of view, we are particularly interested in robust estimation methods, either analytic or learning-based. Finally, in this work we considered only the features obtained from the FOA channels. Nevertheless, the extension to HOA is straightforward, and is planned for coming publications.

6. REFERENCES

- [1] V. Pulkki, "Spatial sound reproduction with directional audio coding," *Journal of the Audio Engineering Society*, vol. 55, no. 6, pp. 503–516, 2007.

- [2] J. Daniel, J.-B. Rault, and J.-D. Polack, “Ambisonics encoding of other audio formats for multiple listening conditions,” in *Audio Engineering Society Convention 105*. Audio Engineering Society, 1998.
- [3] S. Spors, “Extension of an analytic secondary source selection criterion for wave field synthesis,” in *Audio Engineering Society Convention 123*. Audio Engineering Society, 2007.
- [4] J. Merimaa, *Analysis, synthesis, and perception of spatial sound: binaural localization modeling and multichannel loudspeaker reproduction*, Ph.D. thesis, Helsinki University of Technology, 2006.
- [5] T. Rossing (Ed.), *Springer handbook of acoustics*, Springer Science & Business Media, 2007.
- [6] F. Jacobsen, “A note on instantaneous and time-averaged active and reactive sound intensity,” *J. of Sound and Vibration*, vol. 147, no. 3, pp. 489–496, 1991.
- [7] F. Fahy, *Foundations of engineering acoustics*, Elsevier, 2000.
- [8] J. Daniel, *Représentation de champs acoustiques, application à la transmission et à la reproduction de scènes sonores complexes dans un contexte multimédia*, Ph.D. thesis, University of Paris VI, 2000.
- [9] D. Jarrett, E. Habets, and P. Naylor, “3D source localization in the spherical harmonic domain using a pseudointensity vector,” in *18th European Signal Processing Conference (EUSIPCO)*. IEEE, 2010, pp. 442–446.
- [10] S. Kitić and A. Guérin, “TRAMP: Tracking by a Real-time AMbisonic-based Particle filter,” in *LOCATA Challenge Workshop - a satellite event of IWAENC*, 2018.
- [11] D. Pavlidi, S. Delikaris-Manias, V. Pulkki, and A. Mouchtaris, “3D localization of multiple sound sources with intensity vector estimates in single source zones,” in *2015 23rd European Signal Processing Conference (EUSIPCO)*. IEEE, 2015, pp. 1556–1560.
- [12] C. Evers, H. Loellmann, H. Mellmann, A. Schmidt, H. Barfuss, P. Naylor, and W. Kellermann, “The LOCATA Challenge: Acoustic Source Localization and Tracking,” *IEEE Transactions on Audio, Speech and Language Processing*, 2019.
- [13] L. Perotin, R. Serizel, E. Vincent, and A. Guérin, “CRNN-based multiple DoA estimation using acoustic intensity features for Ambisonics recordings,” *IEEE Journal of Selected Topics in Signal Processing*, 2019.
- [14] T. Nakatani, T. Yoshioka, K. Kinoshita, M. Miyoshi, and B.-H. Juang, “Speech dereverberation based on variance-normalized delayed linear prediction,” *IEEE Transactions on Audio, Speech, and Language Processing*, vol. 18, no. 7, pp. 1717–1731, 2010.
- [15] A. Moore, C. Evers, and P. Naylor, “Direction of arrival estimation in the spherical harmonic domain using subspace pseudointensity vectors,” *IEEE/ACM Transactions on Audio, Speech and Language Processing (TASLP)*, vol. 25, no. 1, pp. 178–192, 2017.
- [16] S. Hafezi, A. Moore, and P. Naylor, “Augmented intensity vectors for direction of arrival estimation in the spherical harmonic domain,” *IEEE/ACM Transactions on Audio, Speech and Language Processing (TASLP)*, vol. 25, no. 10, pp. 1956–1968, 2017.
- [17] O. Nadiri and B. Rafaely, “Localization of multiple speakers under high reverberation using a spherical microphone array and the direct-path dominance test,” *IEEE/ACM Transactions on Audio, Speech, and Language Processing*, vol. 22, no. 10, pp. 1494–1505, 2014.
- [18] L. Madmoni and B. Rafaely, “Direction of arrival estimation for reverberant speech based on enhanced decomposition of the direct sound,” *IEEE Journal of Selected Topics in Signal Processing*, vol. 13, no. 1, pp. 131–142, 2018.
- [19] I. Dokmanić, R. Parhizkar, A. Walther, Y. Lu, and M. Vetterli, “Acoustic echoes reveal room shape,” *Proceedings of the National Academy of Sciences*, vol. 110, no. 30, pp. 12186–12191, 2013.
- [20] S. Kitić, N. Bertin, and R. Gribonval, “Hearing behind walls: localizing sources in the room next door with cosparsity,” in *2014 IEEE International Conference on Acoustics, Speech and Signal Processing (ICASSP)*. IEEE, 2014, pp. 3087–3091.
- [21] H. Javed, A. Moore, and P. Naylor, “Spherical microphone array acoustic rake receivers,” in *2016 IEEE International Conference on Acoustics, Speech and Signal Processing (ICASSP)*. IEEE, 2016, pp. 111–115.
- [22] N. Bertin, S. Kitić, and R. Gribonval, “Joint estimation of sound source location and boundary impedance with physics-driven cosparsity regularization,” in *2016 IEEE International Conference on Acoustics, Speech and Signal Processing (ICASSP)*. IEEE, 2016, pp. 6340–6344.
- [23] T. Gerkmann and R. Hendriks, “Unbiased MMSE-based noise power estimation with low complexity and low tracking delay,” *IEEE Transactions on Audio, Speech, and Language Processing*, vol. 20, no. 4, pp. 1383–1393, 2012.